DYNAMIC CRACK PROPAGATION IN WEAK SNOWPACK LAYERS: INSIGHTS FROM HIGH-RESOLUTION, HIGH-SPEED PHOTOGRAPHY

Bastian Bergfeld[1]*, Alec van Herwijnen[1], Jürg Dual[2] and Jürg Schweizer[1]

[1] *WSL Institute for Snow and Avalanche Research SLF, Davos, Switzerland*
[2] *Institute for Mechanical Systems, ETH Zürich, Zürich, Switzerland*

ABSTRACT: To assess the avalanche triggering potential, information on failure initiation and crack propagation is required. While in the past failure initiation has extensively been studied, research focusing on the dynamics of crack propagation only started with the introduction of the Propagation Saw Test (PST) in the mid 2000s. Since then, various studies used particle tracking analysis of high-speed video recordings of PST experiments to gain insight into crack propagation processes, including slab bending, weak layer collapse, crack propagation speed and the frictional behavior after weak layer fracture. Nevertheless, many issues remain unanswered as due to the limited resolution of the videos it thus far was not possible to investigate dynamic processes, especially in the vicinity of the crack tip in the weak layer. We therefore recorded a PST experiment using a powerful portable high-speed camera with a horizontal resolution of 1280 pixels at 10,000 frames per second. By applying a high density speckling pattern on the entire PST column, we then used digital image correlation (DIC) to derive high-resolution displacement and strain fields in the slab, weak layer and substratum. Based on the displacement of the slab, we determined the evolution of weak layer crack speed and compared it to an alternative method where the strain concentration within the weak layer was used. Our results show that crack speed can be derived with both approaches. Hence, our measurement methodology has the potential to provide new insights into the dynamics of sustained crack propagation and crack arrest associated with slab avalanche release.

KEYWORDS: snow avalanche, fracture, crack speed, slab, weak layer, high-speed photography

1. INTRODUCTION

While avalanches come in many different types and sizes, in the following we will focus on dry-snow slab avalanches, as the most difficult to predict and typically the most dangerous. Dry-snow slab avalanche release is the result of a sequence of fracture processes. Failure initiation induced by external loading or the coalescence of sub-critical failures can lead to a localized crack of critical size so that rapid crack propagation starts and the slab-weak layer system becomes unstable. In the subsequent dynamic crack propagation phase the crack travels across the slope as the weak layer fails. Avalanche release then occurs if the gravitational pull on the slab is great enough to overcome frictional resistance to sliding (Schweizer et al., 2003).

For snow, our understanding of the onset of crack propagation has improved within the last decade and models were developed to predict the critical size r_c of a crack within the weak layer when rapid propagation starts. No matter whether a pure shear failure model (McClung, 2011), the anticrack model (Heierli et al., 2008) or the more recent approach by Gaume et al. (2017) is considered to describe r_c, all models rely on the mechanical properties of the slab-weak layer system and do not explicitly consider any time dependency. Whereas a quasi-static assumption is likely appropriate for the onset of crack propagation, the subsequent dynamic phase can be strongly influenced by inertial effects. Hence, time dependency has to be taken into account and the speed of the crack tip becomes an important measure.

In fracture mechanics, it is well known that after the onset of crack propagation, the speed of the

* *Corresponding author address:*
Bastian Bergfeld, WSL Institute for Snow and Avalanche Research SLF, Flüelastrasse 11, CH-7260 DavosDorf, Switzerland
tel: +41 81 4170 354, email: bergfeld@slf.ch

crack tip instantaneously increases to about 10% of the Raleigh wave speed of a material, and it is theoretically limited to a fraction of the Rayleigh wave speed (Marder and Fineberger, 1996). For snow, assuming a shear modulus of 10 MPa, a density of 200 kg m^{-3} and a Poisson's ratio of 0.2, the upper limit is about 180 m s^{-1} and initially the speed should be around 18 m s^{-1}. High-speed photography of Propagation Saw Tests (PST), a fracture mechanical field experiment for snow (Sigrist and Schweizer, 2007; van Herwijnen and Jamieson, 2005) combined with Particle Tracking Velocimetry (PTV) provided new insight into weak layer fracture and crack propagation. Crack propagation speed measurements range from 10 to 30 m s^{-1} (van Herwijnen et al., 2016) and are therefore in line with the theoretical predictions of incipient crack speed. All crack speed measurements in PST experiments are derived from the displacement of the slab by using a threshold for the measured slope normal displacement. Then the speed is calculated based on when subsequent sections of the slab pass this threshold as the crack gradually propagates towards the far end of the PST. Hence, all published crack speed values from PST experiments rely on the same assumption that the slab displacement along the force of gravity, in other words the collapse of the weak layer, occurs simultaneously as the weak layer fractures at the crack tip. An alternative measurement method allowing an independent validation is thus far not available.

Crack speed estimates derived with PTV of PSTs also suffer from methodical limitations. While some videos were taken at frame rates up to 1000 frames per second (fps), most results were obtained at about 120 fps. Assuming a crack propagation speed of 20 m s^{-1} and a 2 m long beam results at best in ten frames during the propagation phase. In combination with the spatial resolution of the PTV, frame speeds were therefore too low to track changes in crack speed along the PST column. In addition, the spatial resolution of the PTV analysis is limited as it relies on black markers inserted into the side wall of the PST. Hence the spatial measurement resolution is limited by the number and spatial density of the markers. There is thus no information within the weak layer, and strain, derived from the spatial derivative of displacement, cannot be estimated reliably with this method. However, such information is of crucial importance to comprehensively study snow fracture leading to avalanche release

2. METHODS

We performed fracture mechanical field experiments based on the PST, recorded high-speed videos of the experiments and used digital image correlation (DIC) to derive high-resolution displacement and strain fields in the slab, weak layer and substratum.

2.1 Field experiment

In March 2018 we performed field experiments above Davos in the Eastern Swiss Alps. On a north-facing 31° steep slope at about 2400 m.a.s.l we performed several PST's that did not propagate to the far end of the beam. To force full propagation in the PST experiments, we therefore added approximately 20 cm of snow (mean density of 250 kg m^{-3}) on the slab. The original slab thickness was 36 cm and consisted of small rounded grains or decomposed and fragmented precipitation particles (mean density of 150 kg m^{-3}). About an hour after adding the snow on the slab, we cut into the weak layer consisting of surface hoar (grain size: 4-8 mm) resulting in a full propagation PST. The PST was 335 cm long and 30 cm wide. One side wall of the PST was speckled with black ink (Figure **1**a) applied with a pump spray. Using a Phantom VEO710 high-speed camera, we filmed the speckled wall of the PST experiment with 10,000 frames per second and a resolution of 1280 × 600 pixel.

2.2 Digital image correlation

Digital image correlation (DIC) is a widely used experimental technique to determine full-field displacements from a sequence of digital images. DIC consists of comparing two digital images of the specimen surface in an un-deformed and deformed state. For the DIC analysis we exported raw images from the captured movie and selected a region of interest (ROI) encompassing the speckled PST wall where the displacement and strain fields were estimated.

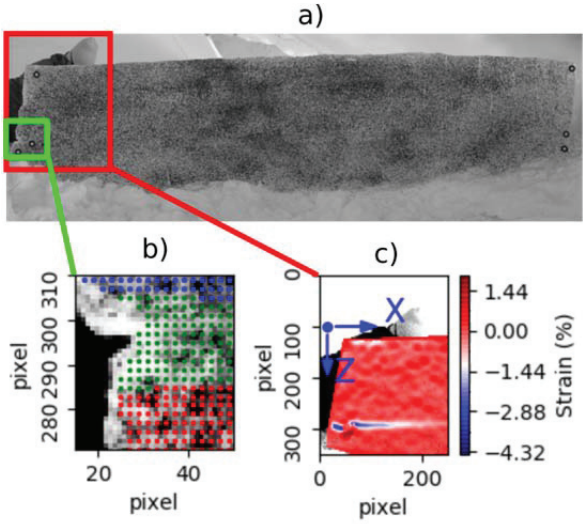

Figure 1: (a) Image of the speckled wall in the PST experiment (b) Close-up showing the centroids of subsets for the slab (blue), weak layer (green) and substratum (red). (c) Measured strain field. The coordinate system used in the DIC analysis is shown in the upper left corner. The strain concentration within the weak layer is clearly visible shortly after crack propagation started

The ROI was further subdivided into subsets and their position was tracked over time. For correlation, displacement and strain calculation we used the DICe software (Turner, 2015) using a subset size of 10 × 10 pixel and a step size of 2 pixels between the subsets. This resulted in a total of 77,146 measurement points (subsets) within the ROI, corresponding to a measurement point every 5.6 mm and every 100 µs. Strains were computed as displacement field gradients within a virtual strain gauge with a window size of 15 × 15 pixel. Finally, measurent points were assigned to the slab, the weak layer and the substratum (blue, green and red dots in Figure **1**b).

2.3 Crack speed

We calculated crack speed with two different methods.

First, we used the method used by van Herwijnen and Jamieson (2005) by selecting a threshold (0.35 mm) for the slope normal displacement $\Delta z(t)$ for every subset in the slab. As the crack propagates through the weak layer, the weak layer collapses and the slab gradually subsides. Hence, displacement curves of subsets from the sawing end of the slab show displacement first and then gradually the subsets towards the far end of the beam (Figure 2a). The time delay Δt between the displacement curves is then used to calculate crack speed. Therefore, the time when Δz of a subset exceeds the threshold value is noted and linked with the x-position of the given subset (blue dots in Figure 3). As crack speed $c = \Delta x/\Delta t$, the crack speed evolution is derived as the slope of linear fits to moving windows (orange dots in Figure 3), which overlap by 90%.

Second, we calculated crack speed by using the slope normal strain in the weak layer (Figure **1**c). The method is essentially the same as for the displacement based crack speed. However, the threshold value for the strain was variable for different subsets in the weak layer as we considered a time frame before the onset of crack propagation and calculated the mean $\bar{\varepsilon}$ and standard deviation std of the slope normal strain for each subset in the weak layer. Based on preliminary results, we then defined the individual threshold as: $\bar{\varepsilon} + 6.5std$.

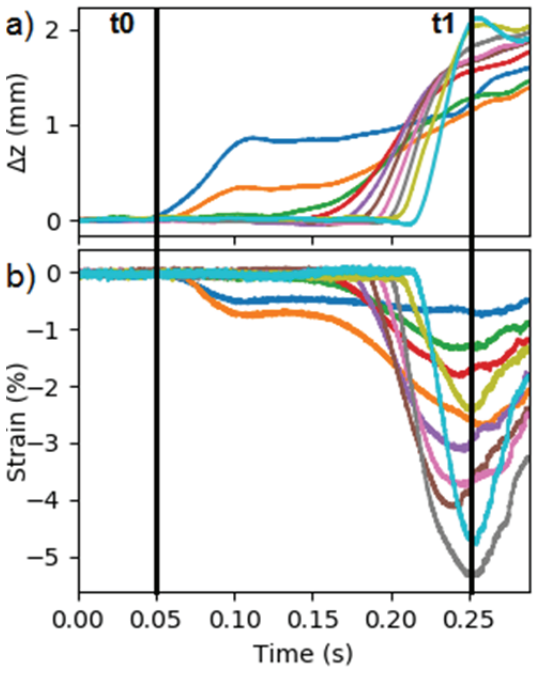

Figure 2: (a) Slope normal displacement of the slab and (b) slope normal strain over the weak layer with time. The different lines correspond to mean displacement or strain at different locations along the PST beam. The vertical black lines indicate the time interval of crack propagation (t0<t<t1).

3. RESULTS AND DISCUSSION

3.1 Displacements and strains

In Figure 2, mean displacement and strain of 34 cm wide columns along the PST beam is shown. The temporal order of the curves also reflects the position of the columns relative to the edge of the PST. Note that the different colors are purely for visual purposes. The slope normal displacement gradually increased from the onset of crack propagation (t_0) up to the point when the crack tip arrived at the far end of the PST (t_1; Figure 2a). Afterwards, the displacement still somewhat increased due to erosion of the crack faces while the slab slid downslope. The collapse (Figure 2a, $t_0 < t < t_1$) was first noticeable in subsets close to the saw and later in subsets towards the far end of the PST.

Figure 3 shows that the displacement threshold was first passed for subsets close to the saw so at small x-positions within the PST, and then towards the far end of the beam. The plateau in the time interval between 0.09 s and 1.15 s suggests that the crack shortly stopped before crack propagation started again. To determine crack speed we choose a moving window containing 4000 subsets (orange dots in Figure 3) and an overlap of 90%.

Similar to the displacement curves in the slab, subsets within the weak layer show zero compressive strain prior to crack propagation (Figure 2b, $t<t_0$) and increasing strain during crack propagation (Figure 2b, $t_0<t<t_1$).

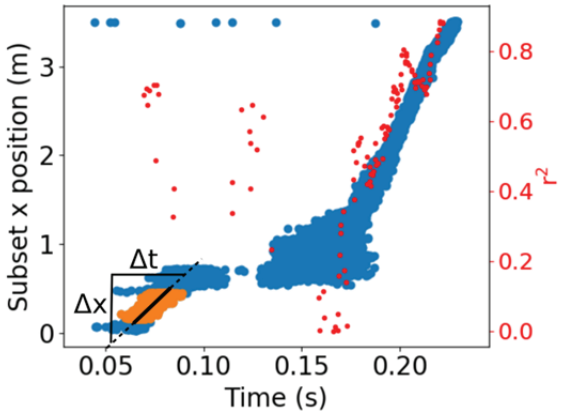

Figure 3: x-position of a subsets with time when the subset exceeds the displacement threshold (blue dots). A linear fit of 4000 subsets (orange dots) determines the crack speed $c = \Delta x/\Delta t$. The red dots indicate the goodness of fit as expressed with the coefficient of determination r^2.

To estimating the crack speed based on strain we applied an individual strain threshold for each subset and derived the speed as the slope of a linear fit for a moving window containing 50 weak layer subsets (overlap 90%). We did not use a fixed threshold value as with the displacement in the slab since the strain is calculated based on the displacement gradient within a strain window of 15 × 15 pixel. This corresponds to a physical size of 4.2 × 4.2 cm^2, which is far larger than the thickness of the weak layer. Hence, the strain window contains the weak layer where strain is expected to be concentrated but also adjacent regions of slab and substratum with low strain. With the present setup it is therefore not possible to estimate absolute values for weak layer strain. Due to the limited thickness of the weak layer and the size of the strain windows, there are far fewer strain measurement points contained in the weak layer than displacement measurement points in the slab. Consequently, the fitting window to derive speed was reduced by two orders of magnitude, leading to less statistical smoothing and more scatter in the crack speed estimates.

3.2 Crack speed

Figure 4 shows the temporal evolution of crack speed during crack propagation in a PST. Both, displacement and strain based methods estimate an initial crack speed of 17 m s^{-1}, before the speed drops to almost zero at x = 40 cm and x = 55 cm, respectively. Thereafter, at x = 1 m, the crack speed increases again up to x = 2.3 m, where it fluctuates around 37 m s^{-1} and 45 m s^{-1} before decreasing again in the last 30 cm of the PST. While both methods show the same qualitative trend, the strain based method resulted in larger speed estimates than the displacement based method. Nevertheless, both methods resulted in crack speed estimates in line with previously reported values from PSTs (10-30 m s^{-1}; van Herwijnen et al., 2016).

The initial decrease in crack speed in our single experiment is difficult to explain. Close inspection of the movie revealed a faint slab fracture that may be the reason for the temporary crack arrest. Yet, it remains even more unclear, why

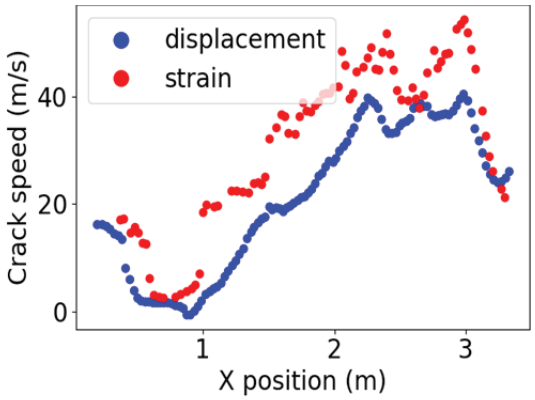

Figure 4: Dynamics of weak layer crack propagation in a PST. In blue, the evolution of crack speed with x-position along the PST beam is based on slab displacement and in red on weak layer strain.

the crack then started again and traveled across the entire PST beam.

The predominantly higher speed values found with the strain based method cannot easily be explained either. Reasons can be manifold. Evaluating this discrepancy in more detail will require a thorough threshold sensitivity analysis and measurement uncertainty estimates.

As we modified the original slab by adding snow on it, our single experiment does not represent a typical PST with full propagation. Nevertheless it shows that both methods can resolve crack speed fluctuations at the scale of a PST.

4. CONCLUSIONS AND OUTLOOK

We recorded a PST experiment using a powerful portable high-speed camera. By applying a high density speckling pattern on the entire PST column, we then used digital image correlation (DIC) to derive the displacement of the slab and the strain across the weak layer. Assuming certain thresholds for slab displacement as well as weak layer strain, we then derived two independent estimates of crack speed .

Our preliminary results show that crack speed can be derived with both approaches and that our measurement methodology will allow measuring changes in crack propagation speed at the scale of a PST beam. While we measured the evolution of strain across the weak layer during dynamic crack propagation, it was not possible to determine the true strain within the weak layer due limitations in the measurement setup. The spatial resolution is still too low since one strain window involves slab or substratum regions adjacent to the weak layer. In the future, we plan to increase the spatial resolution by filming close-ups around the weak layer. Moreover, we will of course record more experiments with either clear crack arrest or full propagation – rather than with seemingly temporary crack arrest as in our single experiment so far.

ACKNOWLEDGEMENT

This project is funded through the Swiss National Science Foundation (grant 200021_16942).

REFERENCES

Gaume, J., van Herwijnen, A., Chambon, G., Wever, N. and Schweizer, J., 2017. Snow fracture in relation to slab avalanche release: critical state for the onset of crack propagation. Cryosphere, 11(1): 217-228.

Heierli, J., van Herwijnen, A., Gumbsch, P. and Zaiser, M., 2008. Anticracks: A new theory of fracture initiation and fracture propagation in snow. In: C. Campbell, S. Conger and P. Haegeli (Editors), Proceedings ISSW 2008, International Snow Science Workshop, Whistler, Canada, 21-27 September 2008, pp. 9-15.

Marder, M. and Fineberger, J., 1996. How things break. Physics Today, 49(9): 24-29.

McClung, D.M., 2011. The critical size of macroscopic imperfections in dry snow slab avalanche initiation. J. Geophys. Res. -Earth Surf., 116(F3): F03003.

Schweizer, J., Jamieson, J.B. and Schneebeli, M., 2003. Snow avalanche formation. Rev. Geophys., 41(4): 1016.

Sigrist, C. and Schweizer, J., 2007. Critical energy release rates of weak snowpack layers determined in field experiments. Geophys. Res. Lett., 34(3): L03502.

Turner, D.Z., 2015. Digital Image Correlation Engine (DICe) Reference Manual. SAND2015-10606 O, National Technology & Engineering Solutions of Sandia.

van Herwijnen, A., Bair, E.H., Birkeland, K.W., Reuter, B., Simenhois, R., Jamieson, B. and Schweizer, J., 2016. Measuring the mechanical properties of snow relevant for dry-snow slab avalanche release using particle tracking velocimetry. In: E. Greene (Editor), Proceedings ISSW 2016. International Snow Science Workshop, Breckenridge CO, U.S.A., 3-7 October 2016, pp. 397-404.

van Herwijnen, A. and Jamieson, B., 2005. High-speed photography of fractures in weak snowpack layers. Cold Reg. Sci. Technol., 43(1-2): 71-82.